Research article

Xiaole Liu, Jie Yuan, Dong Wu, Xiaobin Zou, Qing Zheng, Weina Zhang and Hongxiang Lei*

All-optical targeted drug delivery and real-time detection of a single cancer cell

https://doi.org/10.1515/nanoph-2019-0318
Received August 19, 2019; revised November 8, 2019; accepted November 11, 2019

Abstract: Targeted drug delivery and real-time detection both play an important role for studying the specificity of a single cancer cell and the development of anticancer drugs. However, a method that simultaneously enables safe and efficient targeted drug delivery and noninvasive, free-label cell detection is highly desirable but challenging. Here, we report an all-optical method that combines fiber optical tweezers with laser Raman microspectroscopy, which can achieve targeted drug delivery to a single cancer cell using optical manipulation *in vitro* quickly and accurately by a tapered fiber probe, and simultaneously record the corresponding active characteristics of the targeted cancer cell under the contact of delivered drug through a Raman spectrometer. Using the method, drug delivery and release can be flexibly controlled by turning on/off the trapping laser beam propagating in the fiber, which can avoid the complex systems and is highly autonomous and controllable. Moreover, the detection of cell activity does not require any dye calibration and processing, and it is noninvasive. In addition, for a single suspension cell, optical trapping of the cell using another fiber tip can overcome the low efficiency of targeted drug delivery and the poor stability of the Raman spectrum caused by Brownian motion of the cell. This all-optical method provides a promising approach to conduct pharmacologic studies with the reaction of cancer cell and drugs at the level of a single cell.

***Corresponding author: Hongxiang Lei,** School of Materials Science and Engineering, State Key Laboratory of Optoelectronic Materials and Technologies, Sun Yat-Sen University, Guangzhou 510275, China, e-mail: leihx@mail.sysu.edu.cn. https://orcid.org/0000-0001-9232-937X
Xiaole Liu, Dong Wu, Xiaobin Zou, Qing Zheng and Weina Zhang: School of Materials Science and Engineering, State Key Laboratory of Optoelectronic Materials and Technologies, Sun Yat-Sen University, Guangzhou 510275, China
Jie Yuan: School of Medical Informatics, Daqing Campus, Harbin Medical University, Daqing 163319, China

Keywords: optical tweezers; Raman detection; drug delivery.

1 Introduction

Targeted drug delivery and real-time detection of a single cell are particularly important in the field of cell biology and biomedicine, such as drug development [1–3], tissue engineering [4, 5], genetic engineering [5, 6] and cell heterogeneity [7], especially in testing of drugs [8, 9]. In order to improve the specificity, safety and efficiency of drug delivery, various drug delivery systems have been developed. For example, the chemically powered micro/nanomotors consisting of tiny synthetic devices can be powered by ejected hydrogen bubbles resulting from the chemical reaction between the internal fuel (hydrogen peroxide) and the modified metal nanoparticles on motors [10, 11]. To achieve a nontoxic and fuel-free drug delivery, researchers have explored some physically powered delivery systems [12, 13], such as magnet-actuated, light-driven and ultrasound-propelled systems. For the magnet-actuated system, some magnetic metal compounds such as NdFeB, $CoFe_2O_4$ and $MnFe_2O_4$@$CoFe_2O_4$ were deposited on the drug carriers as power sources, so that the drug carriers can move along the specified direction under a magnetic field regulation [14–16]. The uniqueness of the light-driven system is that the light can be utilized as the tunable energy source to drive the directional movement of drug carriers [17–19], which have demonstrated their potential in targeted drug delivery as a proof of concept. In the systems, some photoactive semiconductors (e.g. TiO_2, silicon) were fabricated as microswimmers [17, 18] and nanomotors [19]. They can move only in the presence of light, which was mainly based on light-induced self-electrophoresis, and they can stop at places of interest when the light is switched off. In other light-controlled systems for targeted drug delivery, light can only be used for releasing loaded drugs [20, 21]. The ultrasound-propelled systems use the pressure gradient generated by the geometric asymmetry of drug carriers under an action of the ultrasound to control the movement of drug carriers [22, 23]. The above delivery systems

require complex structures or additional modification of drug carriers to respond to the action of various physical fields. Besides, these physical methods are generally suitable for overall control of all drug carriers in the system, so they cannot be applied for precise manipulation of a single drug carrier or quantitative delivery of multiple drug carriers to a single cell. Moreover, to verify the effectiveness of the targeted drugs in the above systems, the activity of cancer cells was detected by the complex methods of chemical labeling, fluorescence imaging and metabolite detection. Therefore, there is an urgent demand to explore a safe, convenient, flexible and efficient method that can achieve both a controllable targeted drug delivery and real-time detection of a single cancer cell.

Tapered fiber prober (TFP), as a simple, flexible and powerful tool, has been widely applied in the noncontact optical manipulation of dielectric micro-/nanoparticles, bacteria, cells and even DNA with good stability and high efficiency [24, 25], and it has also been demonstrated to have an advantage of controllable delivery of micro-/nanoparticles and cells in three-dimensional space [26–29]. For example, a single yeast cell has been stably trapped and driven to targeted regions by a TFP [26]; stable trapping and three-dimensional flexible movement of microparticle or cell chains was achieved using a TFP by optical binding [27]; multiple cells of different types were connected with each other and patterned 1D periodic cell structures by an abrupt TFP, which can also be flexibly moved to targeted regions [28]. Based on the modified TFP (assembling microlenses on the TFP), nanoparticles and biological cells were selectively trapped and detected by collecting the backscattering signals of the trapped objects in real time [29]. The modified TFP was also applied to the imaging of a single cell by collecting the fluorescence signals in real time at subwavelength spatial resolution [25]. Therefore, applying the optical manipulation technology of fiber optical tweezers to the targeted drug delivery and stable trapping of a single suspension cancer cell will be very promising. Even more excitingly, the above experiment for optical manipulation can be carried out under a Raman microscope, so real-time detection of a single cancer cell will be simultaneously obtained by monitoring the Raman spectrum of the cell. The noninvasive optical detection tool can obtain the active characteristics of cancer cells without extra fluorescent dyes or chemical makers, and it has been used extensively in the identification of health, apoptosis and death of cancer cells [30, 31]. Therefore, the combination of optical manipulation technology and laser Raman microspectroscopy is highly desired. In 2019, Stocker et al. combined microfluidics, traditional optical tweezers and Raman microspectroscopy to achieve an automated sorting of the isotope-probing-labeled microbial cells [32]. However, to our knowledge, no existing application combining the fiber optical tweezers with Raman microspectroscopy for targeted drug delivery and real-time detection of a single cancer cell has been reported before.

Thus, we present an all-optical method based on fiber optical tweezers and laser Raman microspectroscopy. In the method, drug carriers, one or several mesoporous silica microparticles loaded with an anticancer drug – doxorubicin (MMD), can be stably trapped under an action of optical force and then delivered to a targeted adherent cancer cell accurately and quickly only using one TFP. Here, doxorubicin can initiate the formation of hydroxyl radicals after reduction of free doxorubicin, and these hydroxyl radicals can damage cellular membranes by lipid peroxidation or damage cellular DNA [33]. At the same time, the changes of the active characteristics of the cancer cell can be detected real-timely by Raman microscopy. For a single suspension cancer cell, it is necessary to add another TFP to trap the cell and thus avoid Brownian motion of the cell. The proposed all-optical method combines several intriguing features, namely convenient and flexible structure, controllable drug loading capacity, safe and efficient drug delivery, controllable drug release, and noninvasive, free-label and real-time detection of the cell.

2 Experiment

2.1 Fabrication of TFP

The TFP was fabricated with a flame-heating technique from a commercial single-mode optical fiber (connector type: FC/PC, core diameter: 9 μm, cladding diameter: 125 μm; Corning Inc.). In the first step, a fiber stripper (Shanghai Connet Fiber Optics Co., Ltd., Shanghai, China) was used to strip the buffer and polymer jacket of fiber to obtain a bare fiber with a 2.5 cm length and a 125 μm diameter, and then the fiber was sheathed with a glass capillary (Hangzhou Fuqiang Chemical Instrument Co., Ltd., Hangzhou, Zhejiang Province, China) (inner diameter: ~0.9 mm, wall thickness: ~0.1 mm, length: ~120 mm) to protect the fiber from breakage and warping, and ensure the stability of the fiber movement. In the second step, both sides of the bare fiber were clamped by two thin-tipped tweezers to make the midpoint of the bare fiber be heated by the outer flame of an alcohol lamp for approximately 50 s to reach its melting point (see Supplementary Figure S1); then the heated fiber was drawn with an

initial speed of about 0.5 mm/s, and the fiber diameter was decreased from 125 μm to approximately 15 μm over a 1.5 mm length to form a gradual taper. This was followed by increasing the drawing speed to 5–10 mm/s, which can form an abruptly tapered region with a different size we need; the fiber was then broken with a tapered tip. The tapered tip at the end was formed by the surface tension of the melting fiber. In the last step, the extra fine tip of the tapered fiber was wiped carefully with a piece of lens cleaning tissue with some alcohol.

2.2 Treatment for cells

HeLa cells were cultured in Dulbecco's modified Eagle's medium with 10% fetal bovine serum (FBS), 1% glutamine and 1% penicillin streptomycin are all purchased from Guangzhou Hengyan Biotechnology Co., Ltd., Guangzhou, Guangdong Province, China. Myelogenous leukemia tumor cells (K562 cell) with STR identification were purchased from Procell Life Science & Technology Co., Ltd. K562 cells were cultured in RPMI Medium 1640 basic with 10% FBS, 1% glutamine and 1% penicillin streptomycin. Both types of cells were incubated in the incubator at 37°C and with 5% CO_2. The day before the experiment, HeLa cells were seeded on a cover glass (15 mm in diameter), and then incubated in a CO_2 incubator for 12 h. At the beginning of the experiment, the HeLa cells were washed four times with phosphate-buffered saline (PBS), and the cells were taken on the cover glass on a slide of the translation stage. Then the immediately formulated MMD suspension was dripped into the cell medium. In the case of K562 cells, that needs to be diluted with PBS.

2.3 Characterization of the mesoporous silica microparticles and preparation of MMDs

The mesoporous silica microparticles with a 3 μm diameter were purchased from Wuhan Huake Microtechnology Co., Ltd. The mesoporous silica microparticles were characterized via scanning electron microscopy (SEM) at an acceleration voltage of 15 kV and a transmission electron microscope (TEM) at an acceleration voltage of 120 kV. Ultra-thin sectioning of samples was required before testing TEM. For preparation of MMDs, 3 mg dry mesoporous silica was mixed with 3 ml of doxorubicin PBS solution (2 mg ml^{-1}), and an ultrasonic treatment of 5 min was needed to obtain a good dispersion. The solution was then stirred in a magnetic stirrer for 24 h. After stirring, the solution was divided into two equal parts and centrifuged at 3000 RPM, which was followed by drawing out the supernatant and washing the sample three times with PBS. Finally, the sample was dried in a vacuum drying cabinet for 12 h to get dry MMDs.

2.4 Raman microscope for the detection of cells

All Raman spectra were obtained using a Horiba XploRA PLUS Confocal Raman microscope (Horiba, Kyoto, Japan). We used a 50×/0.5 NA objective lens, both for illuminating the cells and for collecting the Raman signal. A 532 nm laser with a power of 10 mW was used for excitation. Each Raman spectrum detection was performed with an integral time of 5 s and an accumulation number of 5, which could be averaged to reduce an error.

3 Results and discussion

3.1 Experimental schematic

Figure 1A shows the schematic of the experimental setup. All the experiments were carried out under a Raman microscope with a charge-coupled device camera and objective lens. A personal computer interfacing the microscope was used to observe and record the experimental process. The substrate of the cell medium was placed on the translation stage of the Raman microscope, and a rocker can precisely control the movement of the translation stage. A TFP (see methods for fabrication) sheathed partly by a glass capillary was inserted into the cell medium using a tunable six-axis micromanipulator (Kohzu Precision Co., Ltd., resolution: 50 nm). A 980-nm laser beam (Beijing wavicle laser Co., Ltd., Beijing, China) with an optical power of 20 mW, which exhibits relatively low absorption for biological specimens [28], was launched into the TFP to create a stable optical trap. By precisely moving the TFP to approach the drug carriers [mesoporous silica microparticles loaded with an anticancer drug – doxorubicin (MMD)] sequentially, one or several drug carriers can be trapped near the tip of the TFP by the optical gradient force. Then, the trapped drug carriers can be delivered to the adherent cancer cell accurately, and finally they can be released by turning off the 980-nm laser source. For a single suspension cell, another TFP with an additional 980-nm laser beam and micromanipulator is necessary to trap the cell stably (see the dotted box). To

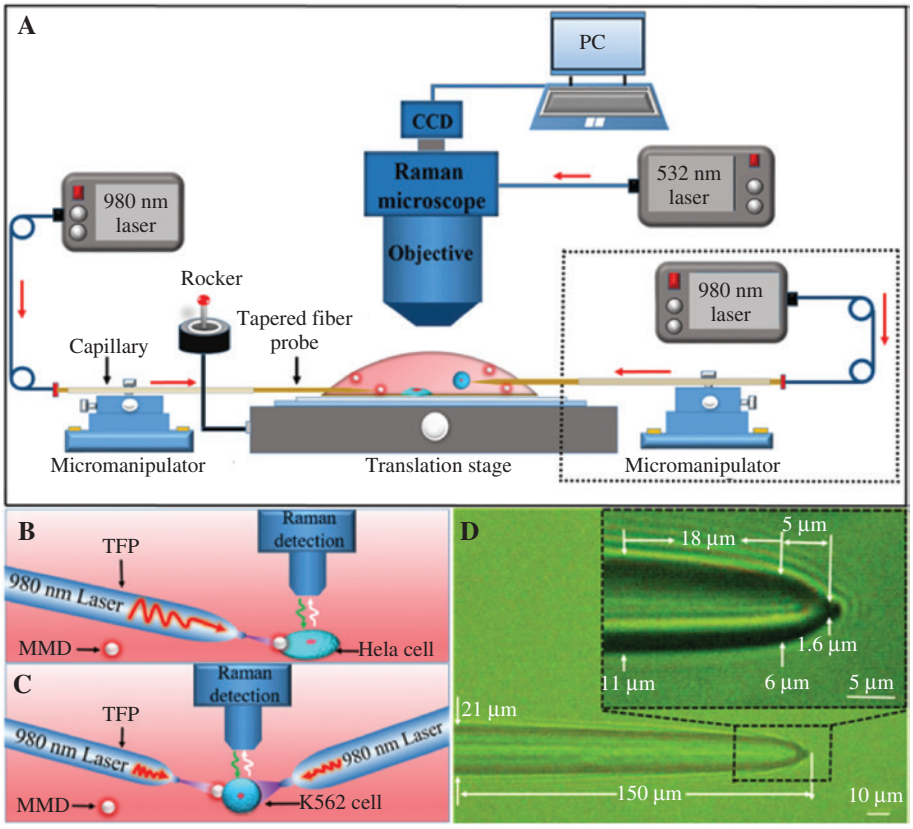

Figure 1: Schematic of the experiments.
(A) Schematic of the experimental setup. The red arrows indicate the direction of the input laser beam. (B) Schematic of targeted drug delivery and Raman detection for a single HeLa cell. The red arrow indicates the input 980 nm laser beam used for trapping MMD, and the green and white arrows indicate a 532 nm excitation laser beam and the Raman scattered light, respectively. (C) Schematic of targeted drug delivery and Raman detection for a single K562 cell. Another TFP was added to trap the K562 cell. The red arrow indicates the input 980 nm laser beam used for trapping the MMD or K562 cell, and the green and white arrows indicate a 532 nm excitation laser beam and the Raman scattered light, respectively. (D) Optical microscope image of the TFP used in experiment.

verify the effectiveness of the drug delivery, the activity of the cancer cell can be detected real-timely by monitoring the Raman spectrum of the cell. Here, a 532-nm laser beam was coupled to the Raman microscope to excite Raman signals of the targeted cell. Figure 1B and C presents schematics of targeted drug delivery and real-time detection for a single adherent cancer cell (HeLa cell as an example) and a single suspension cancer cell (K562 cell as an example), respectively. Figure 1D shows an optical micrograph of TFP used for the targeted drug delivery in the experiment. The diameter of the TFP was first gradually decreased from 11 to 6 μm with a length of 18 μm and then rapidly decreased from 6 to 1.6 μm over a length of 5 μm, and finally ended with a taper in the form of a parabola. Here, it should be emphasized that the geometry of the fiber tip is critical to trap and manipulate micro-objects, because the tip of TFP acts as a high NA objective that can focus the laser beam to further generate a strong optical force for the micro-objects.

3.2 Characterization of the mesoporous silica microparticles

Due to a good biocompatibility, high drug loading and release ability, and easily modified feature, mesoporous silica microparticles have been widely used in the development of anticancer drug carriers [3, 34]. Figure 2A shows the SEM image of mesoporous silica microparticles with diameters of 3 μm used in the experiment. In order to observe the morphology of pore structure, the TEM image of mesoporous silica microparticle is shown in Figure 2B, and a large number of pore structures are relatively evenly distributed in the sphere plane. Here, it is needed to point out that the TEM image in Figure 2B just shows a small broken piece of the mesoporous silica microparticle, because the microparticle has to be treated with ultrathin sectioning due to a limit of sample thickness in the TEM detection. To obtain a specific information of the drug-carrying ability of the mesoporous silica microparticles,

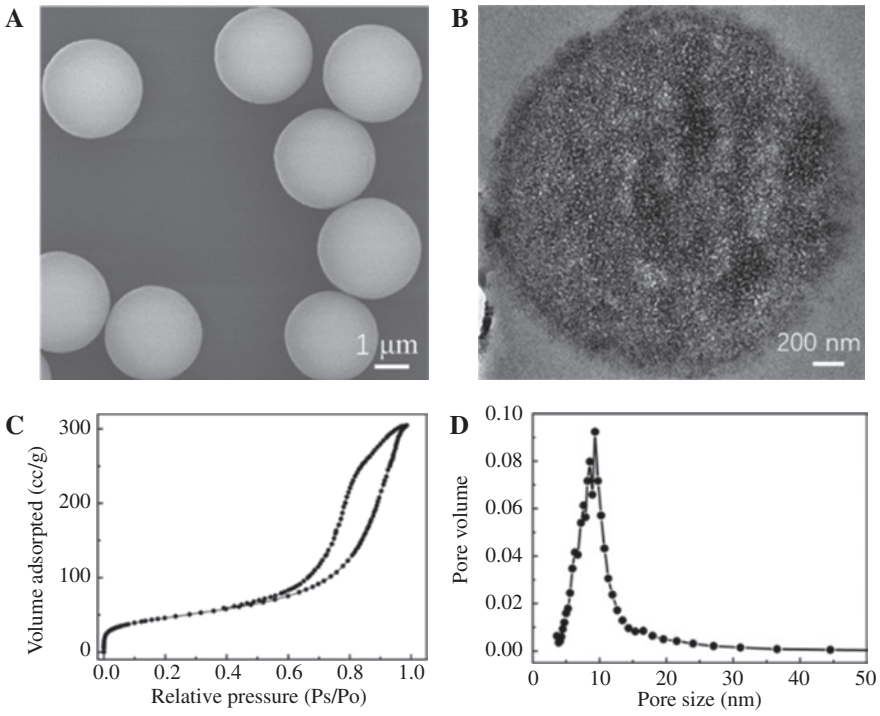

Figure 2: Characterization of the mesoporous silica microparticles.
(A) SEM image of the mesoporous silica microparticles. (B) TEM image of a small broken piece of the mesoporous silica microparticle. (C) N_2 adsorption/desorption isotherm of the mesoporous silica microparticles. (D) Barrett-Joyner-Halenda desorption pore size distribution curve of the mesoporous silica microparticles.

Figure 2C and D shows the N_2 adsorption/desorption isotherm and the Barrett-Joyner-Halenda desorption pore size distribution curve of the microparticles, respectively. Through calculation, the results show that the surface area, pore size and pore volume of the microparticle are 166 m^2/g, 9 nm and 0.5 ml/g, respectively (see method for characterization). It indicates that the mesoporous silica microparticles used in the experiments have a high loading capacity. Based on the measured pore volume of the mesoporous silica microparticle in Figure 2C and D, the drug dose loaded in a mesoporous silica particle can be estimated to be about 11.92×10^{-12} g, which agrees with the experimental value (see details in Section 2 of Supplementary Material).

3.3 Targeted drug delivery and real-time detection of a single HeLa cell

HeLa cell, as an adherent cancer cell, has been widely used in the experiments of targeted drug delivery. Taking a HeLa cell as the targeted cell in our experiment (see the activity demonstration of cells before the experiment in Section 3 of Supplementary Material), Figure 3A–H shows the experimental process for delivering MMDs to a HeLa cell. To avoid the drug impact on the targeted cell in advance, in our experiment, the MMDs were highly diluted into the cell suspension in order to ensure that no MMDs exist within a range of 1000 μm of the targeted HeLa cell. The tip of the TFP in Figure 1A was prepared for the following experiment. Once a 980-nm laser beam was launched into the TFP with an optical power of 20 mW, a focused optical field generated at the end of the TFP. By moving the TFP to approach an MMD, the MMD can be trapped due to an action of optical force with a direction toward the end of the TFP. Then, by adjusting the fiber micromanipulator or the sample translation stage, the trapped MMD can be translated in three-dimensional space and thus delivered into the targeted cell. Figure 3B–D shows that a trapped MMD was delivered to the position with distances of 115, 27 and 0 μm from the targeted cell. The whole delivery process of the first MMD took 15 s, and the average delivery speed was calculated to be about 100 μm/s, which is faster than 19.6, 48.5 and 59 μm/s achieved by the mentioned chemically or physically powered delivery system [11, 19, 20]. Moreover, it is worth to note that a more stable trapping and faster delivery rate of MMDs can be obtained with a higher laser power. But, accordingly, a higher photothermal effect can also be generated, which can lead to the instability of liquid environment and is

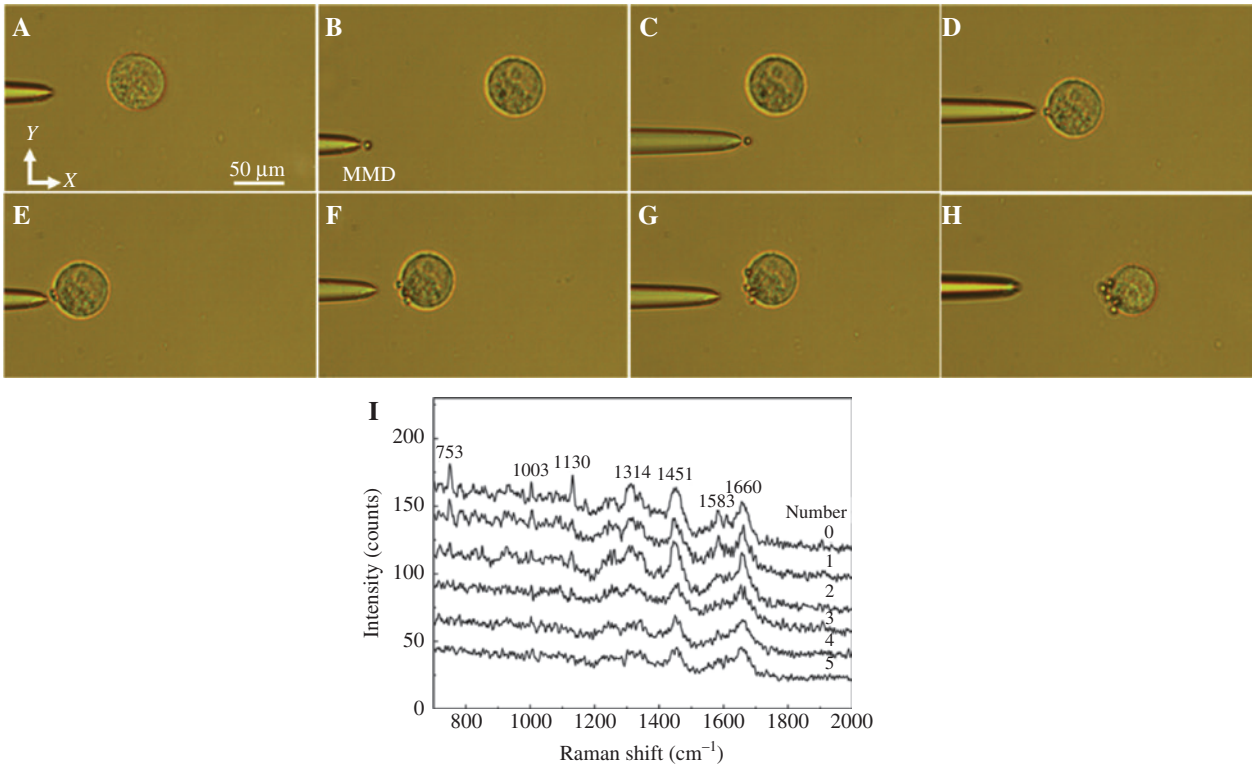

Figure 3: The optical microscope images of the delivery process of MMDs and the corresponding Raman spectrum of the targeted HeLa cell. (A) A HeLa cell was selected as the targeted cell, and no MMDs exist within a range of 1000 μm of the targeted HeLa cell. The tip of the TFP was moved near the targeted cell to prepare for trapping and delivering MMDs. (B–D) The first trapped MMD was delivered to the position with distances of 115, 27 and 0 μm from the targeted cell, respectively. (E–H) An additional four MMDs were successively trapped and delivered into the targeted cell by the TFP in the same time intervals (5 min). (I) The corresponding Raman spectrum of the targeted HeLa cell recorded real-timely by the Raman microscope.

also harmful to biological specimens. In our experiment, to avoid an obvious photothermic effect, the laser power is generally set as less than 40 mW [28]. When the delivery process was completed, the trapped MMD can be released by turning off the laser source. Thus, the anticancer drug (doxorubicin) will autonomously diffuse into the cell and then interacts with the cell. To investigate an impact of drug doses on the cell, more MMDs (five particles as examples) were successively trapped and delivered into the targeted cell by the above method with the same time intervals (5 min), as shown in Figure 3E–H. Meanwhile, the effect of each MMD on the targeted cell was detected and recorded real-timely through the Raman microscope, as shown in Figure 3I. To ensure the enough drug release, the Raman spectrum was recorded after every MMD had been released for 5 min. Moreover, all Raman spectra averaged from 5 spectra. The time of collecting spectrum is very short (~5 s), which was ignored in our experiment. According to the literature, Raman peaks of HeLa cells can be assigned to several vibrational modes [35–38]. The Raman peaks at 753, 1130, 1314 and 1583 cm^{-1} can be assigned to the Pyrrole breathing mode ν_{15}, C–N stretching of protein, C–H deformation of protein and $C_\alpha C_m$ asymmetric stretching in cytochrome c, respectively. The other Raman peaks appearing at 1003, 1451 and 1660 cm^{-1} can be assigned to the ring breathing mode of phenylalanine, CH_2 deformation and Amide-I vibrational mode of peptide bonds, respectively. For comparison, the Raman spectrum of the targeted cell with no MMDs nearby was also detected and recorded. It is corresponding to the curve with number = 0 in Figure 3I, which shows a good activity of the targeted cell. With the delivery of the first MMD and the release of drugs, the second Raman spectrum with number = 1 was detected at the contact point between the targeted cell and the first MMD. There was only a slight decrease at the peak of 1130 cm^{-1}, which indicates that only cytochrome c changed a little under the influence of the first MMD in 5 min. For the third Raman spectrum with number = 2, the signal intensity presents an obvious attenuation at the peaks of 753, 1003 and 1583 cm^{-1}, which indicates that the cytochrome c and proteins of the targeted cell were both affected. For the fourth Raman spectrum with number = 3,

the Raman peaks at 1314 and 1451 cm^{-1} were attenuated, which indicates that the condition of phospholipids in the targeted cell started to change. As the fourth MMD was delivered to the targeted cell (Figure 3G), the corresponding Raman signals with number = 4 were recorded, which shows that only the peaks at 1003, 1130, 1451 and 1660 cm^{-1} are slightly obvious and the cell activity has been greatly challenged. After the fifth MMD was delivered to the targeted cell, the corresponding Raman spectrum recorded with number = 5 in Figure 3I shows that only the peaks at 1451 and 1660 cm^{-1} exist, which indicates a significant apoptosis of the targeted cell. Here, the curve with number = 5 in Figure 3I is the Raman spectrum recorded in 25 min. The above results indicate that severe apoptosis occurred in the targeted cells after the drug doses of five MMDs were successively released into the targeted cell every 5 min.

Benefited from the abruptly tapered shape of the TFP, the laser beam output from the TFP is more concentrated along the fiber axis, which allows multiple MMDs to be trapped by the strong optical gradient force along the fiber axis [28]. Specially, the trapped MMD at the end of the TFP can acts as a microlens to focus the transmission light output from itself again, and the refocused light can continue to generate an enough optical force to trap the next MMD again. Thus, more MMDs can be trapped and connected. Therefore, the above TFP can be used to realize not only an accurate, quick and noncontact delivery of a single MMD, but also quantitative delivery of multiple MMDs at one time, which is beneficial to achieve a controllable drug delivery capacity. Taking five MMDs as an example, Figure 4A–D shows the delivery process of the five MMDs at one time. In Figure 4A, no MMDs exist around the targeted HeLa cell and the TFP was adjusted to the same plane with the targeted cell to prepare for the trapping and delivering experiment. With a 980-nm laser beam launched into the TFP with an optical power of 30 mW, five MMDs were successively trapped by moving the fiber micromanipulator or the translation stage to make the TFP near the five MMDs one by one. Subsequently, continuing to move the TFP, the five trapped MMDs were delivered to the position with distances of 130, 65 and 0 μm from the targeted cell, respectively, as shown in Figure 4B–D. The delivery process of the five MMDs from Figure 4B–D took 21 s, and the average delivery speed was calculated to be about 60 μm/s. After the five MMDs were released to the targeted cell, the relations of the drug doses versus the therapeutic time were investigated by detecting and recording the Raman spectrum of the targeted cell every 5 min, as shown in Figure 4E. The first Raman spectrum at time = 0 was recorded immediately once the five MMDs were released, which shows that the activity of targeted cell is great at the beginning. The Raman spectrum at time = 5 min shows that besides a slight decrease at the peak of 1130 cm^{-1}, the peaks at 753, 1314 and 1583 cm^{-1} present a significant decline. Compared with the impact of one MMD on the HeLa cell in 5 min (Figure 3I), the changes of cytochrome c were more significant here. The third Raman spectrum at time = 10 min shows that the peaks at 753, 1314 and 1660 cm^{-1} were decreased, which indicates that cytochrome c and peptide bonds in proteins were further changed. As time = 15 min, the two slightly obvious peaks at 1451 and 1660 cm^{-1} and three weak peaks at 1003, 1130 and 1314 cm^{-1} existed, which indicates that the activity of targeted cell was severely affected. When time is 20 min, the Raman spectrum was similar to that of the cell with five MMDs successively released every 5 min (see the curve with number = 5 in Figure 3I); it means the

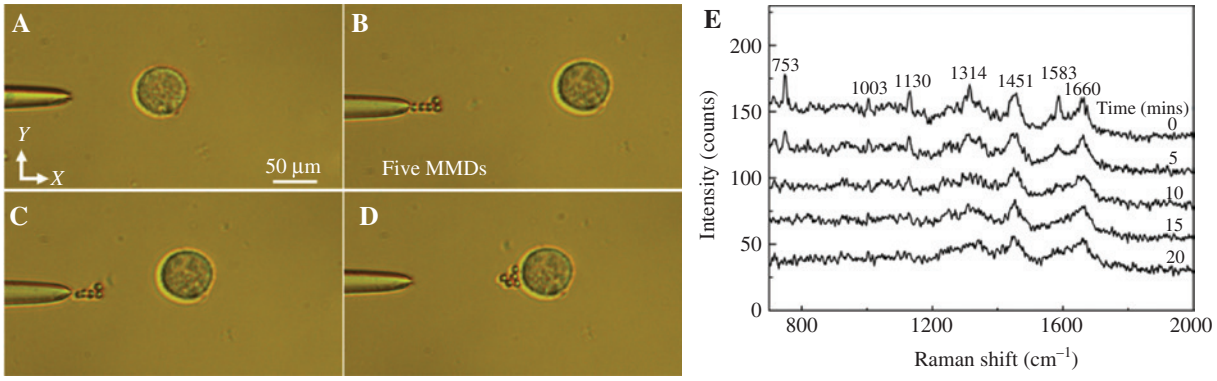

Figure 4: The optical microscope images of delivering five MMDs and the Raman spectrum of the targeted HeLa cell over time.
(A) No MMDs exist within a range of 1000 μm of the targeted HeLa cell and the TFP was prepared for the following trapping and delivering experiment. (B–D) The five trapped MMDs were delivered to the position with distances of 130, 65 and 0 μm from the targeted cell, respectively. (E) The Raman spectrum of the targeted cell with the different therapeutic time.

targeted cell underwent a severe apoptosis. The above results indicate that severe apoptosis occurred in the targeted cells after the drug doses of five MMDs were one-timely released into the targeted cell in 20 min, which is more effective than that with five MMDs successively released into the targeted cell every 5 min.

To confirm that the changes in spectra are attributable to the drug and not the interaction of the unloaded microspheres, an additional experiment was performed (see Section 4 in Supplementary Material). The results show that the influence of mesoporous silica microparticles can be ignored in our work and the reductions in Raman spectra were resulted from the drug. In the above experiments, only reduction in the intensities of the specific peaks was recorded and there is no biological effect described. To further prove the apoptosis of targeted cells after the drug release, an additional experiment was performed by injecting a trypan blue staining assay. The results show that the targeted cell was stained blue, and it means that the apoptosis occurred in the targeted cells after the drug release. The details are described in Supplementary Material (Section 5).

3.4 Targeted drug delivery and real-time detection of a single K562 cell

For suspension cells, due to their disadvantages of Brownian motion, they require an extra assist of complex equipment to implement the targeted drug delivery and a stable Raman detection. Benefited from the development of optical manipulation technology, the optical fiber has been proven to be a more flexible, convenient and efficient tool to limit Brownian motion of the suspension cells and can further to obtain physical or chemical information of the trapped suspension cells. In our experiment, taking a single suspension K562 cell with a 30 μm diameter as a sample, it was first trapped using another TFP with a large tapered angle as shown in Figure 5A. Here, the TFP with a large tapered angle is very crucial for trapping the large size cells stably [28]. The optical power of the 980-nm laser beam for trapping the K562 cell was 30 mW, which is not harmful to the cell [25]. Similar to the above experiment, at the beginning of the recording experiment (Figure 5A), no active MMDs exist around the targeted K562 cell and the TFP at the left was adjusted to the same plane with

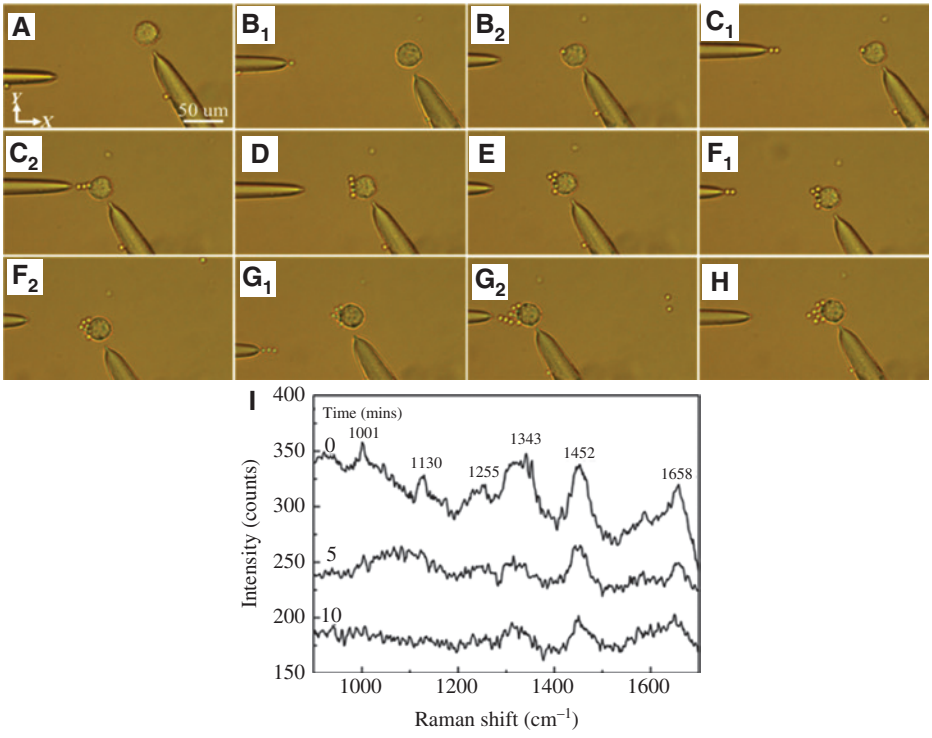

Figure 5: Optical microscope images of delivering 10 MMDs to a single K562 cell and the Raman spectrum of the targeted cell over time. (A) A single K562 cell was trapped by the right TFP and the left TFP was ready for the trapping and delivery of MMDs. (B_1 and B_2) The delivery of the first MMD. (C_1 and C_2) The delivery of the second and third MMDs at one time. (D) The fourth MMD was delivered to the targeted cell. (E) The fifth MMD was delivered to the targeted cell. (F_1 and F_2) The delivery of the sixth and seventh MMDs at one time. (G_1 and G_2) The delivery of the eighth, ninth and tenth MMDs at one time. (H) The completed delivery of 10 MMDs. (I) The Raman spectrum of the K562 cell over time.

the targeted cell to prepare for the following trapping and delivering experiment of MMDs. Keeping the K562 cell stably trapped in the whole process, multiple MMDs (10) were successively trapped and then delivered into the trapped K562 cell in a similar way as the above, as shown in Figure 5B–H. Figure $5B_1$ and B_2 shows the delivery process of the first MMD; Figure $5C_1$ and C_2 shows the simultaneous delivery process of the second and third MMDs; Figure 5D and E shows the delivery of the fourth and fifth MMD, respectively; Figure $5F_1$ and F_2 shows the simultaneous delivery of sixth and seventh MMDs; Figure $5G_1$ and G_2 shows the delivery process of the eighth, ninth and tenth MMDs simultaneously; Figure 5H shows the finished delivery of 10 MMDs. Here, it should be noted that to avoid the trapped K562 cell from getting out of the trap due to the environmental disturbance, the movement of the translation stage cannot be too fast. In the experiment, the moving velocity was controlled below 80 μm/s. In order to detect the effects of 10 MMDs on the targeted K562 cell, the Raman detection was performed on the targeted cell every 5 min staring from the delivery completion of 10 MMDs, as shown in Figure 5I. Compared with the HeLa cell, the new Raman peaks at 1255 and 1343 cm^{-1} of K562 cells can be assigned to Amide III and C-H deformation [39, 40]. From the first Raman spectrum at time = 0 in Figure 5I, we can see that the activity of the targeted cell was in a good condition. At time = 5 min, the peaks at 1130, 1255, 1343 cm^{-1} decline severely and the state of the targeted cell changed significantly. At time = 10 min, the peaks at 1001, 1343, 1658 cm^{-1} for the Raman spectrum show sharp declines too, which indicates that the targeted cell underwent apoptosis significantly. The above results indicate that a single suspension cancer cell needs to be first trapped by adding another TFP for the further delivery of drugs and a severe apoptosis occurred in the targeted cell with the release of the drug doses of 10 MMDs in 10 min.

To confirm that the changes in spectra are attributable to the drug and not the laser beam, an additional experiment was performed (see Section 4 in Supplementary Material). The results show that the photothermal damage of the laser beam on the K562 cell can be ignored in our work and the reductions in Raman spectra were resulted from the drug.

3.5 Numerical analysis

The above experiments proved the accurate and quick delivery of one or multiple MMDs to a single adherent cell and a single suspension cell, respectively, only by a TFP. To deeply investigate the TFP's trapping stability and delivery capability for one or multiple MMDs, a theoretical model was built with a finite element method using COMSOL Multiphysic (COMSOL Co., Ltd., Beijing, China). Figure 6A and B shows the simulated energy density of the 980-nm laser beam output from the TFP, with one and five MMDs trapped at the TFP tip, respectively. In the simulation, the shape of the TFP was set as the same as that in Figure 1D and the MMD was set as a ball with a diameter of 3 μm. The refractive indices of the TFP, cell medium and MMDs were set to be 1.44, 1.33, and 1.45, respectively. The optical power of the 980-nm laser beam was normalized to be 1 W. Obviously, the light was highly concentrated, confined and propagated along the trapped MMDs (the optical fiber axis). From the distribution of energy density, the optical forces acted on the MMDs can be obtained by taking the integral of the time-independent Maxwell stress tensor $\langle \mathbf{T}_M \rangle$ on the external surface of the MMDs. $\mathbf{F_o}$ can be expressed as [27]

$$\mathbf{F_o} = \oint (\langle \mathbf{T}_M \rangle \cdot \mathbf{n}) \mathrm{d}S, \tag{1}$$

where the integration is performed over a closed surface S surrounding the MMDs, $\mathbf{n}$ is the surface normal vector of S and $\langle \mathbf{T}_M \rangle$ is the time-independent Maxwell stress tensor, which is given by

$$\langle \mathbf{T}_M \rangle = \mathbf{D}\mathbf{E}^* + \mathbf{H}\mathbf{B}^* - \frac{1}{2}\left(\mathbf{D}\cdot\mathbf{E}^* + \mathbf{H}\cdot\mathbf{B}^*\right)\mathbf{I}, \tag{2}$$

where $\mathbf{D}$ and $\mathbf{H}$ are the electric displacement and magnetic field, respectively; $\mathbf{E}^*$ and $\mathbf{B}^*$ are the complex conjugates of the electric field $\mathbf{E}$ and magnetic flux field $\mathbf{B}$, respectively; $\mathbf{I}$ is the isotropic tensor.

Figure 6C and D shows the energy density along the optical fiber axis (x-axis) corresponding to Figure 6A and B, respectively. The coordinate origin ($x = 0$) starts at the end of TFP. Along the positive direction of the x-axis, the energy density is abruptly decreased in Figure 6C, which indicates that a large optical gradient exists along the fiber axis. More specifically, two peaks at $x = 2.2$ and 5.8 μm appear in Figure 6C, which corresponds the two focuses of the light output from the TFP and from the MMD, respectively. It further indicates that the light is highly confined and propagated along the MMD, and thus more MMDs can be trapped and connected. For an example, in Figure 6D, a very high peak appears yet at the end of the fifth MMD and the optical intensity is 72.9% of the highest optical intensity, which also indicates the strong focus ability of five MMDs and low loss of propagating light along the MMD chain. According to Eqs. (1) and (2), the total optical force F_o exerted on the trapped MMD in Figure 6A was –12.58 pN. The optical forces F_o exerted on five MMDs in

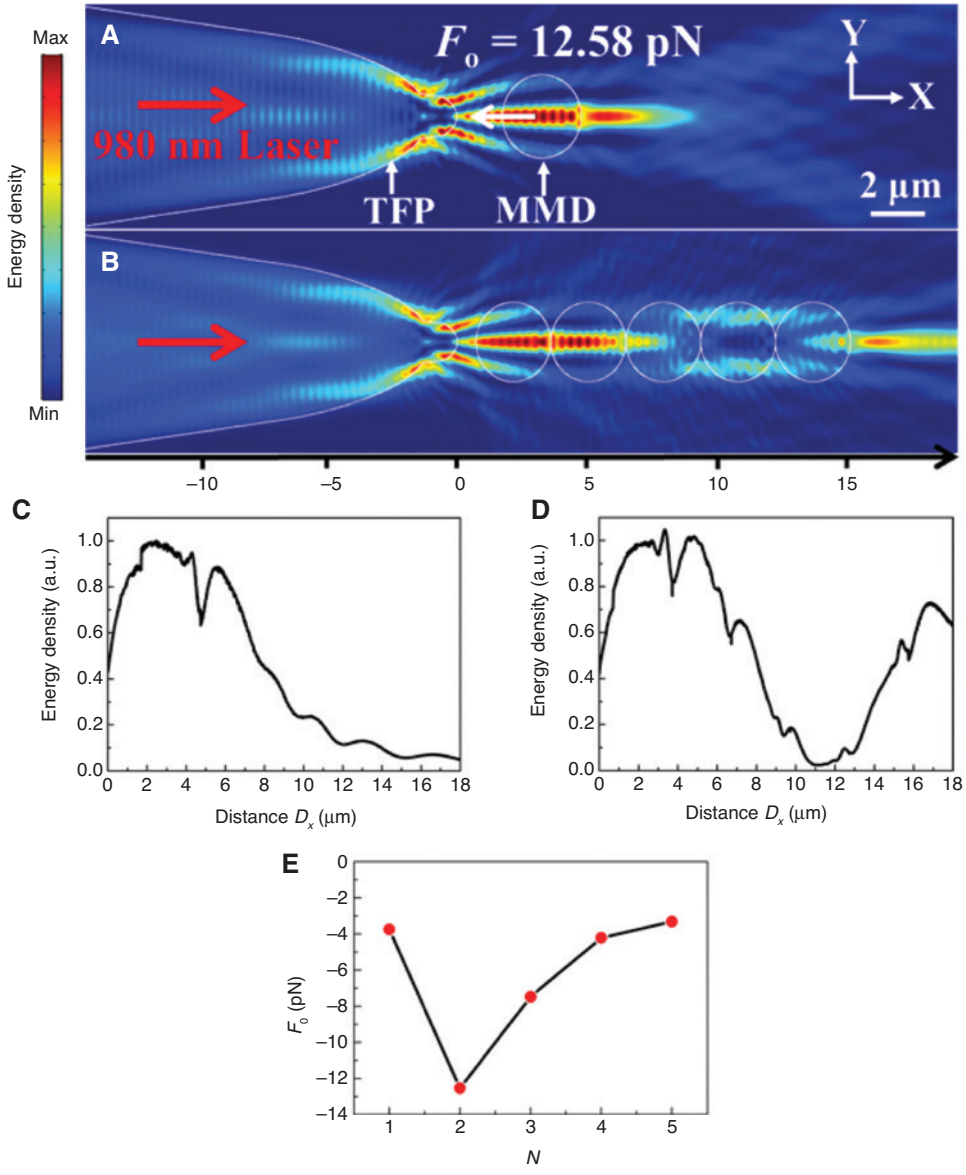

Figure 6: Simulation and calculation results.
(A) Simulated energy density distribution output from the TFP with an MMD trapped at the focus of the TFP. (B) Simulated energy density distribution output from the TFP with five MMDs trapped along the optical fiber axis. (C) Energy density along the optical fiber axis in (A). (D) Energy density along the optical fiber axis in (B). (E) The calculated optical force F_o acted on the five MMDs by the TFP.

Figure 5B were calculated to be –3.75, –12.54, –9.48, –7.21 and –6.32 pN, respectively, as shown in Figure 6E. This proves that the one and five MMDs can be stably trapped at the end of the TFP under the actions of optical forces, which agrees with the above experimental results.

During the delivery process of the trapped MMD, an extra viscous force can be exerted on the MMD, which may result in the trapping instability. However, in our experiment, the effect can be ignored. To demonstrate this, the viscous force acted on the trapped MMD in the delivery process was calculated by Stokes' drag formula:

$$F = 6\pi r\eta v \tag{3}$$

where $r = 1.5$ μm is the MMD radius, $\eta = 8.9 \times 10^{-4}$ Pa·s is the dynamic viscosity of PBS and v is the moving velocity of the trapped MMD. When $v = 100$ μm/s corresponding to that of the above experiment in Figure 3, the viscous force was calculated to be 2.52 pN, which is smaller than the acted optical trapping force. So, in the delivery process, the MMD was yet trapped stably. Therefore, the proposed method for the targeted drug delivery of MMD to a single cancer cell is reliable.

4 Conclusion

In summary, a convenient and efficient all-optical method combining fiber optical tweezers and Raman microspectroscopy has been experimentally demonstrated for the targeted drug delivery and real-time detection of a single cancer cell. One or multiple MMDs can be stably trapped and then delivered to a single cancer cell quickly and accurately using one TFP, which makes the drug loading capacity controllable. Moreover, the delivery rate and the drug release can also be controlled by changing the moving rate of the fiber micromanipulator or translation stage and by turning off the laser source, respectively. The effects of the drug doses on the targeted cell were recorded by detecting the Raman spectrum of the targeted cell real-timely without extra fluorescent dyes or chemical makers. The results show that the drug doses with five MMDs that were one-timely released into the targeted cell in 20 min can make the targeted adherent cancer cell undergo a severe apoptosis. Additionally, this method has been easily extended to a single suspension cancer cell by adding another TFP. The proposed all-optical method provides a new approach for the drug research of cancer cells at a single cell level.

5 Supplementary material

The supplementary material is available online on the journal's website or from the author.

Acknowledgments: The authors thank Fei Peng from the School of Materials Science and Engineering, Sun Yat-Sen University for experimental assistance. This work was supported by National Natural Science Foundation of China (NSFC) (11974435) and the Guangdong Natural Science Foundation (2018A030313498).

References

[1] Bertrand N, Wu J, Xu X, Kamaly N, Farokhzad OC. Cancer nanotechnology: the impact of passive and active targeting in the era of modern cancer biology. Adv Drug Deliv Rev 2014;66:2–25.
[2] Zhou Y, Quan G, Wu Q, et al. Mesoporous silica nanoparticles for drug and gene delivery. Acta Pharm Sin B 2018;8:165–77.
[3] Castillo RR, Lozano D, González B, et al. Advances in mesoporous silica nanoparticles for targeted stimuli-responsive drug delivery: an update. Expert Opin Drug Deliv 2019;16:415–39.
[4] Shi J, Votruba A, Farokhzad OC, Langer R. Nanotechnology in drug delivery and tissue engineering: from discovery to applications. Nano Lett 2010;10:3223–30.
[5] Tibbitt MW, Dahlman JE, Langer R. Emerging frontiers in drug delivery. J Am Chem Soc 2016;138:704–17.
[6] Li X, He Q, Shi J. Global gene expression analysis of cellular death mechanisms induced by mesoporous silica nanoparticle-based drug delivery system. ACS Nano 2014;8:1309–20.
[7] Xin H, Xu R, Li B. Single upconversion nanoparticle-bacterium cotrapping for single-bacterium labeling and analysis. Small 2017;13:1603418.
[8] Senapati S, Mahanta AK, Kumar S, Maiti P. Controlled drug delivery vehicles for cancer treatment and their performance. Signal Transduct Target Ther 2018;3:1–19.
[9] Rosenblum D, Joshi N, Tao W, Karp JM, Peer D. Progress and challenges towards targeted delivery of cancer therapeutics. Nat Commun 2018;9:1–12.
[10] Sattayasamitsathit S, Kou H, Gao W, et al. Fully loaded micromotors for combinatorial delivery and autonomous release of cargoes. Small 2014;14:2830–3.
[11] Peng F, Tu Y, Hest JCM, Wilson DA. Self-guided supramolecular cargo-loaded nanomotors with chemotactic behavior towards cells. Angew Chem 2015;127:11828–31.
[12] Reinišová L, Hermanová S, Pumera M. Micro/nanomachines: what is needed for them to become a real force in cancer therapy? Nanoscale 2019;11:6519–32.
[13] Peng F, Tu Y, Wilson DA. Micro/nanomotors towards in vivo application: cell, tissue and biofluid. Chem Soc Rev 2017;46:5289–310.
[14] Qiu Y, Tong S, Zhang L, et al. Magnetic forces enable controlled drug delivery by disrupting endothelial cell-cell junctions. Nat Commun 2017;8:15594.
[15] Liu M, Pan L, Piao H, et al. Magnetically actuated wormlike nanomotors for controlled cargo release. ACS Appl Mater Interfaces 2015;7:26017–21.
[16] Chen W, Cheng CA, Zink JI. Spatial, temporal, and dose control of drug delivery using noninvasive magnetic stimulation. ACS Nano 2019;13:1292–308.
[17] Zheng J, Dai B, Wang J, et al. Orthogonal navigation of multiple visible-light-driven artificial microswimmers. Nat Commun 2017;8:1438.
[18] Wang J, Xiong Z, Zhan X, et al. A silicon nanowire as a spectrally tunable light-driven nanomotor. Adv Mater 2017;29:1701451.
[19] Sridhar V, Park BW, Sitti M. Light-driven Janus hollow mesoporous TiO_2-Au microswimmers. Adv Funct Mater 2018;28:1704902.
[20] Wu Z, Lin X, Zou X, Sun J, He Q. Biodegradable protein-based rockets for drug transportation and light-triggered release. ACS Appl Mater Interfaces 2015;7:250–5.
[21] Wang T, Jiang H, Wan L, et al. Potential application of functional porous TiO_2 nanoparticles in light-controlled drug release and targeted drug delivery. Acta Biomater 2015;13:354–63.
[22] Lu X, Soto F, Li J, Li T, Liang Y, Wang J. Topographical manipulation of microparticles and cells with acoustic microstreaming. ACS Appl Mater Interfaces 2017;9:38870–6.
[23] Garcia-Gradilla V, Sattayasamitsathit S, Soto F, et al. Ultrasound-propelled nanoporous gold wire for efficient drug loading and release. Small 2014;10:4154–9.
[24] Gao D, Ding W, Nieto-Vesperinas M, et al. Optical manipulation from the microscale to the nanoscale: fundamentals, advances and prospects. Light Sci Appl 2017;6:e17039.

[25] Li Y, Xin H, Zhang Y, et al. Living nanospear for near-field optical probing. ACS Nano 2018;12:10703–11.
[26] Xin H, Xu R, Li B. Optical trapping, driving, and arrangement of particles using a tapered fibre probe. Sci Rep 2012;2:818.
[27] Xin H, Xu R, Li B. Optical formation and manipulation of particle and cell patterns using a tapered optical fiber. Laser Photon Rev 2013;7:801–9.
[28] Xin H, Li Y, Li B. Controllable patterning of different cells via optical assembly of 1D periodic cell structures. Adv Funct Mater 2015;25:2816–23.
[29] Li Y, Xin H, Liu X, et al. Trapping and detection of nanoparticles and cells using a parallel photonic nanojet array. ACS Nano 2016;10:5800–8.
[30] Kanna B, Offerhaus HL, Windbergs M, Otto C. Raman microscopy for cellular investigations – from single cell imaging to drug carrier uptake visualization. Adv Drug Deliv Rev 2015;89:71–90.
[31] Managò S, Zito G, Luca ACD. Raman microscopy based sensing of leukemia cells: a review. Opt Laser Technol 2018;108:7–16.
[32] Lee KS, Palatinszky M, Pereira FC, et al. An automated Raman-based platform for the sorting of live cells by functional properties. Nat Microbiol 2019;4:1035–48.
[33] Keizer HG, Pinedo HM, Schuurhuis GJ, Joenje H. Doxorubicin (adriamycin): a critical review of free radical-dependent mechanisms of cytotoxicity. Pharmac Ther 1990;47:219–31.
[34] Croissant JG, Fatieiev Y, Almalik A, Khashab NM. Mesoporous silica and organosilica nanoparticles: physical chemistry, biosafety, delivery strategies, and biomedical applications. Adv Healthc Mater 2018;7:1700831.
[35] Hamada K, Fujita K, Smith NI, et al. Raman microscopy for dynamic molecular imaging of living cells. J Biomed Opt 2008;13:044027.
[36] Palonpon AF, Sodeoka M, Fujita K. Molecular imaging of live cells by Raman microscopy. Curr Opin Chem Biol 2013;17:708–15.
[37] Jiang X, Jiang Z, Xu T, et al. Surface-enhanced Raman scattering-based sensing in vitro: facile and label-free detection of apoptotic cells at the single-cell level. Anal Chem 2013;85:2809–16.
[38] Buckmaster R, Asphahani F, Thein M, Xu J, Zhang M. Detection of drug-induced cellular changes using confocal Raman spectroscopy on patterned single-cell biosensors. Analyst 2009;134:1440–6.
[39] Yu Y, Lin JQ, Lin D, et al. Leukemia cells detection based on electroporation assisted surface-enhanced Raman scattering. Biomed Opt Express 2017;8:4108–21.
[40] Perozziello G, Candeloro P, Grazia AD, et al. Microfluidic device for continuous single cells analysis via Raman spectroscopy enhanced by integrated plasmonic nanodimers. Opt Express 2016;24:A180–90.

Supplementary Material: The online version of this article offers supplementary material (https://doi.org/10.1515/nanoph-2019-0318).